Earth and Planetary Science Letters 584 (2022) 117516

Contents lists available at ScienceDirect

Earth and Planetary Science Letters

www.elsevier.com/locate/epsl

No modern Irrawaddy River until the late Miocene-Pliocene

Tara N. Jonell [a,b,c,*], Liviu Giosan [d], Peter D. Clift [c], Andrew Carter [e], Lisa Bretschneider [f], Ed C. Hathorne [f], Marta Barbarano [g], Eduardo Garzanti [g], Giovanni Vezzoli [g], Thet Naing [h]

[a] School of Geographical and Earth Sciences, University of Glasgow, Glasgow G12 8QQ, UK
[b] School of Earth and Environmental Sciences, The University of Queensland, St. Lucia 4101 QLD, Australia
[c] Department of Geology and Geophysics, Louisiana State University, Baton Rouge, LA 70803, USA
[d] Geology and Geophysics, Woods Hole Oceanographic Institution, Woods Hole, MA 02540 USA
[e] Department of Earth and Planetary Sciences, Birkbeck College, London WC1E 7HX, UK
[f] GEOMAR, Helmholtz Centre for Ocean Research Kiel, Wischhofstr. 1-3, 24148 Kiel, Germany
[g] Laboratory for Provenance Studies, Department of Earth and Environmental Sciences, Università di Milano-Bicocca, Piazza della Scienza 4, 20126 Milano, Italy
[h] Department of Geology, Pathein University, Pathein, Myanmar

ARTICLE INFO

Article history:
Received 24 May 2021
Received in revised form 28 February 2022
Accepted 22 March 2022
Available online 4 April 2022
Editor: A. Webb

Keywords:
provenance
sediment
Irrawaddy
zircon
isotope geochemistry
petrography

ABSTRACT

The deposits of large Asian rivers with unique drainage geometries have attracted considerable attention due to their explanatory power concerning tectonism, surface uplift and upstream drainage evolution. This study presents the first petrographic, heavy mineral, Nd and Sr isotope geochemistry, and detrital zircon geochronology results from the Holocene Irrawaddy megadelta alongside modern and ancient sedimentary provenance datasets to assess the late Neogene evolution of the Irrawaddy River. Contrary to models advocating a steady post-middle Miocene river, we reveal an evolution of the Irrawaddy River more compatible with regional evidence for kinematic reorganization in Myanmar during late-stage India-Asia collision. Quaternary sediments are remarkably consistent in terms of provenance but highlight significant decoupling amongst fine and coarse fraction $^{87}Sr/^{86}Sr$ and ε_{Nd} due to hydraulic sorting. Only well after the late Miocene do petrographic, heavy mineral, isotope geochemistry, and detrital zircon U–Pb results from the trunk Irrawaddy and its tributaries achieve modern-day signatures. The primary driver giving rise to the geometry and provenance signature of the modern Irrawaddy River was regional late Miocene ($\leq$10 Ma) basin inversion coupled with uplift and cumulative displacement along the Sagaing Fault. Middle to late Miocene provenance signatures cannot be reconciled with modern river geometries, and thus require significant loss of headwaters feeding the Chindwin subbasin after ~14 Ma and the northern Shwebo subbasin after ~11 Ma. Large-scale reworking after ~7 Ma is evidenced by modern Irrawaddy River provenance, by entrenchment of the nascent drainage through Plio-Pleistocene inversion structures, and in the transfer of significant sediment volumes to the Andaman Sea.

1. Introduction

The Ayeyarwady River, historically known as the Irrawaddy, drains ~420,000 km^2 of SE Asia and delivers to the Andaman Sea one of the highest sediment fluxes in the world (~364 ± 60 × 10^6 t yr^{-1}; Robinson et al., 2007). Since its initiation as a through-flowing river by the late Oligocene to earliest Miocene (Licht et al., 2016; Zhang et al., 2019), the Irrawaddy has infilled the ~900 km-long trough referred to as the Central Myanmar Basin (CMB). The Holocene Irrawaddy delta, the last in a series of prograding deltas, remains one of the last unexplored Asian megadeltas in terms of provenance and drainage evolution. This study presents petrography, heavy mineral, Nd and Sr isotope geochemistry (<2 μm and >2 μm), and detrital zircon U–Pb geochronology data from two drill cores penetrating the Holocene megadelta down to the late Pleistocene flooding surface (Fig. 1; Giosan et al., 2018). New data are evaluated against provenance datasets for the modern river, the late Neogene ancestral Irrawaddy sediment-routing system, and major SE Asian bedrock domains to infer how compositions evolved through space and time. We assess the extent to which hydraulic sorting influences compositional variability and if this, at all, impacts provenance interpretations. Lastly, we elucidate key

* Corresponding author at: School of Geographical and Earth Sciences, University of Glasgow, Glasgow G12 8QQ, UK.
E-mail address: tara.jonell@glasgow.ac.uk (T.N. Jonell).

https://doi.org/10.1016/j.epsl.2022.117516

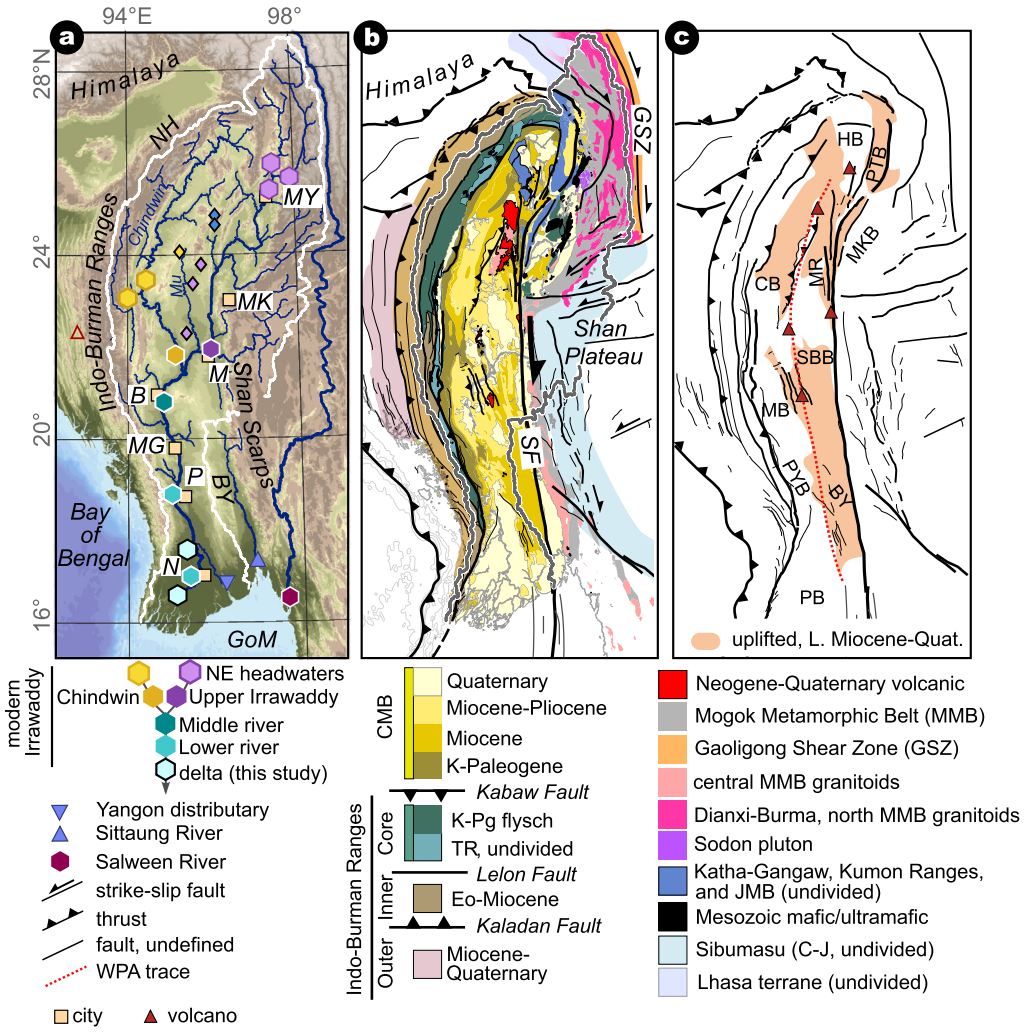

Fig. 1. The Irrawaddy drainage. (A) Irrawaddy River with delta core and modern river samples locations. Samples from Minwun Ranges and Mu River catchment as diamonds; (B) Regional geology (Myanmar Geosciences Society, 2017; Zhang et al., 2012). (C) Uplift distribution of CMB after Sloan et al. (2017) labelled with major Cenozoic subbasins and depocenters. Abbreviations: B–Bagan; BY–Bago Yoma uplift; CB–Central or Chindwin Basin; CMB–Central Myanmar Basin; DB–Dianxi-Burma; GSZ–Gaoligong Shear Zone; HB–Hukawng Basin; JMB–Jade Mines Belt; M–Mandalay; MB–Minbu (Salin) Basin; MG–Magway; MR–Minwun Ranges; MY–Myitkyina; MKB–Myitkyina-Kathaw Basin; N–Nyaungdoung; NH–Naga Hills; P–Pyay; PB–Pathein Basin; PYB–Pyay Basin; SBB–Shwebo Basin; SF–Sagaing Fault. (For interpretation of the colors in the figure(s), the reader is referred to the web version of this article.)

time intervals over which the drainage evolved in response to tectonism.

2. Geological setting

The Irrawaddy Basin is divided into three N/S-trending domains. The easternmost domain, the Shan Plateau, exposes Neoproterozoic-Paleozoic sedimentary rocks intruded by Cambrian to Mesozoic granitoids (Bender, 1983). The second domain, including the Mogok Metamorphic Belt (MMB) and Shan Scarps, is a narrow zone of high-grade metamorphic rocks with Permian to Miocene granitic intrusions continuing northward to the Dianxi-Burma (DB) and Gaoligong regions along the Sino-Burmese border (Socquet and Pubellier, 2005; Zhang et al., 2012).

The Indo-Burman Ranges (IBR) mark the third domain forming the present-day margin between the Indian and Eurasian plates. The IBR are a Mesozoic-Cenozoic accretionary prism, including Triassic schists and slices of Mesozoic ophiolite. Triassic-Paleogene meta-volcaniclastic rocks comprise the IBR Core that is thrust over the CMB (i.e., Maurin and Rangin, 2009). Cretaceous-Eocene metasedimentary rocks form the Inner IBR, with Miocene and younger rocks in the Outer IBR (Aitchison et al., 2019; Allen et al., 2008; Arboit et al., 2021; Naing et al., 2014). The IBR emerged as a topographic barrier adjacent to the ancestral Irrawaddy drainage by the middle Oligocene (Licht et al., 2018), if not the Oligo-Miocene boundary (Najman et al., 2020).

Widespread granitic intrusions delineate two parallel magmatic belts through Myanmar and into Eastern Himalayan Syntaxis. Significant debate exists regarding their development and relationship to nearby Himalayan and SE Asian arcs (i.e., Licht et al., 2020; Lin et al., 2019). Granitoids exposed in the DB and the MMB display Late Cretaceous to early Miocene ages related to their multiphase magmatic and thermal history (i.e., Bertrand et al., 2001; Lamont et al., 2021; Socquet and Pubellier, 2005). Based on their ages, isotopic and geochemical affinities, granitoids in the northern MMB and DB have been correlated northward to the Bomi-Chayu batholiths of the Eastern Himalaya (Lin et al., 2019). The second belt, the Wuntha-Popa Arc, intrudes through the CMB and yields

U–Pb ages clustering at 108–90 Ma, 69–64 Ma, and 46–32 Ma (Licht et al., 2020; Zhang et al., 2019). Several Quaternary volcanoes punctuate the CMB, with less developed magmatic centers extending offshore.

Ongoing India-Asia convergence transfers considerable motion through Myanmar to the Andaman Sea. The primary structure accommodating this hyper-oblique motion is the ~1400-km dextral Sagaing Fault, connecting the Andaman Sea with the Eastern Himalayan Syntaxis. The age and total displacement of the Sagaing Fault remain controversial. Estimates for total displacement range from ~100 km since 5 Ma (Bertrand and Rangin, 2003) to >400 km with older fault-initiation age (Mitchell, 1993). Recent detrital zircon U–Pb evidence from the synkinematic North Minwun Basin (Fig. 1A, C) suggests initiation of dextral motion by the mid-Oligocene (~28–27 Ma), with ~486 km displacement since then (Morley and Arboit, 2019). Structures distributed through the IBR (Bender, 1983; Maurin and Rangin, 2009), CMB (Pivnik et al., 1998; Zhang et al., 2021), and Shan Plateau (Bertrand and Rangin, 2003) accommodate the remainder of India-Eurasia motion. Many predate the Sagaing Fault and likely influenced its early evolution. Late Miocene (<10 Ma) transpression induced thrust faulting and folding that inverted sections of the CMB, including the Bago Yoma, or Pegu Range (Pivnik et al., 1998).

The CMB hosts a thick (≤15 km) succession of Upper Cretaceous-Recent shallow-marine to fluvio-deltaic sedimentary rocks deposited within numerous subbasins that altogether record the evolution of the nascent Irrawaddy drainage (Fig. 2). The contemporaneous Wuntha-Popa Arc broadly separates western forearc and eastern retroarc troughs (Mitchell, 1993). Although variable, Late Cretaceous-Eocene subsidence within subbasins affected total sediment accommodation, eastern and western successions broadly share a similar tectonic evolution (Licht et al., 2016; Thein and Maung, 2017). Paleocurrent and facies analysis indicate that the CMB was open to the Bay of Bengal through the Eocene and much of the Oligocene before emergence of the IBR as a semi-continuous topographic barrier (Allen et al., 2008; Arboit et al., 2021; Licht et al., 2018). By the mid-Oligocene to earliest Miocene, large longitudinal drainages formed the first semblance of an ancestral Irrawaddy system that reached ~23° N in the western trough (Licht et al., 2013; Najman et al., 2020). Following the end of a major Oligo-Miocene transgression, continental clastic sediment infilled the CMB and prograded southward. Only after the mid-late Miocene do freshwater fluvial sediments prograde south of Pyay (18.5° N) into the Pathein Basin embayment (Bender, 1983).

3. The Irrawaddy River

The Irrawaddy River today is characterized by two main tributaries that merge south of Mandalay (~22° N): the Chindwin and Upper Irrawaddy. The Chindwin, draining only the IBR and the west CMB trough, yields ~50–60% of the total sediment flux to the lower river (Garzanti et al., 2016). The Upper Irrawaddy supplies the remaining 40–50% from modern headwaters flowing out from the Eastern Himalayan Syntaxis, past the DB and MMB, before tracing the Sagaing Fault to Mandalay. The trunk Irrawaddy forms near the city of Bagan (Fig. 1) and flows south between the IBR and Bago Yoma. The modern Irrawaddy delta apex begins 270 km from the Andaman Sea at ~18° N. The youngest Ayeyarwady lobe, partly explored in this study, has built out past a promontory formed by the IBR only in the last ~1000 years (Giosan et al., 2018). It is suspected that the advancing delta blankets a broad paleovalley incised into the shelf during glacial lowstands.

The modern drainage can be divided into five geographic sectors that coincide with major CMB subbasins: the NE Irrawaddy headwaters, the Upper Irrawaddy tributary in the Shwebo subbasin, the Chindwin tributary in the Chindwin subbasin, the middle trunk river downstream of the Chindwin-Upper Irrawaddy confluence (~22° N) in the Minbu subbasin, a lower trunk river downstream of Pyay in the Pyay subbasin, and the postglacial delta in the Pathein subbasin. Neogene sedimentary rocks, once part of the Chindwin and Shwebo subbasins (Arboit et al., 2021; Zhang et al., 2019), are also present within the modern Mu River, sandwiched between the Chindwin and Upper Irrawaddy.

Three neighboring rivers supply sediment to the Gulf of Mottama (Martaban): 1) the Sittaung River that drains the Shan Scarps along a paleovalley existing before Miocene inversion (Thein and Maung, 2017); 2) the Yangon River, an abandoned delta distributary eroding uplifted Miocene basin fill (Giosan et al., 2018); and 3) the Salween (Thanlwin, Nu) River that flows from the Tibetan Plateau through the Gaoligong Shear Zone and across the Shan Plateau before reaching the Andaman Sea.

4. Materials and methods

This work presents the first multi-method provenance results from the Pleistocene-Holocene Irrawaddy megadelta. New data are integrated with published petrographic, heavy mineral ($N = 49$; Tables S2–S3), Sr and Nd isotope-geochemistry ($N = 113$; Table S4), and detrital zircon U–Pb geochronology ($n = 8296$; Tables S5–S6) datasets from the Cretaceous-Miocene CMB and modern Irrawaddy River to track the spatio-temporal evolution of the Irrawaddy drainage. We build from several foundational provenance studies establishing initiation of a through-flowing river by the early Neogene, and here follow the evolution of the nascent Irrawaddy through the late Neogene and into the Quaternary.

Two scientific drill cores penetrating down to the pre-deltaic Pleistocene flooding surface recovered material from the middle (IR1) and apex (IR2) of the Irrawaddy Delta in 2016 and 2017 (Giosan et al., 2018). Core lithostratigraphy (Fig. 3) and radiocarbon dating of organic materials indicate an Uppermost Pleistocene-Holocene delta established over Upper Pleistocene fluvial sands and gravels. Full sampling details in Table S1.

4.1. Petrography and heavy minerals

Framework petrography and heavy mineral analyses were conducted at the University of Milano-Bicocca on eight sand samples. A quartered fraction of each sample was impregnated with araldite epoxy and cut into a standard thin section. Petrographic analysis counted 400–500 points under the microscope according to the Gazzi-Dickinson method (Ingersoll et al., 1984). Metamorphic grains were classified according to protolith composition and metamorphic rank (Garzanti and Vezzoli, 2003). From a split aliquot of the 15–500 μm size window obtained by wet sieving, heavy minerals were recovered after centrifuging in Na-polytungstate (2.90 g/cm^3) and partial freezing with liquid nitrogen. For each sample, ≥200 transparent heavy minerals were grain-counted by the area method (Galehouse, 1971). Median grain size was determined by sieving and by ranking and visual comparison in thin section with in-house standards of sieved $\phi/4$ classes. Results are presented in Tables S2–S3 together with published modern and Neogene datasets. Quantitative statistical analysis of petrographic and heavy mineral results was conducted by principle component analysis (PCA) using the R 'provenance' package (Vermeesch et al., 2016). Compositions were evaluated using a Bray-Curtis dissimilarity matrix and reduced into two dimensions (i.e., biplot) for visualization. The compositional biplot (Gabriel, 1971) allows compositional discrimination among multivariate observations (samples, as points) while indicating relationships among variables (phases, as rays).

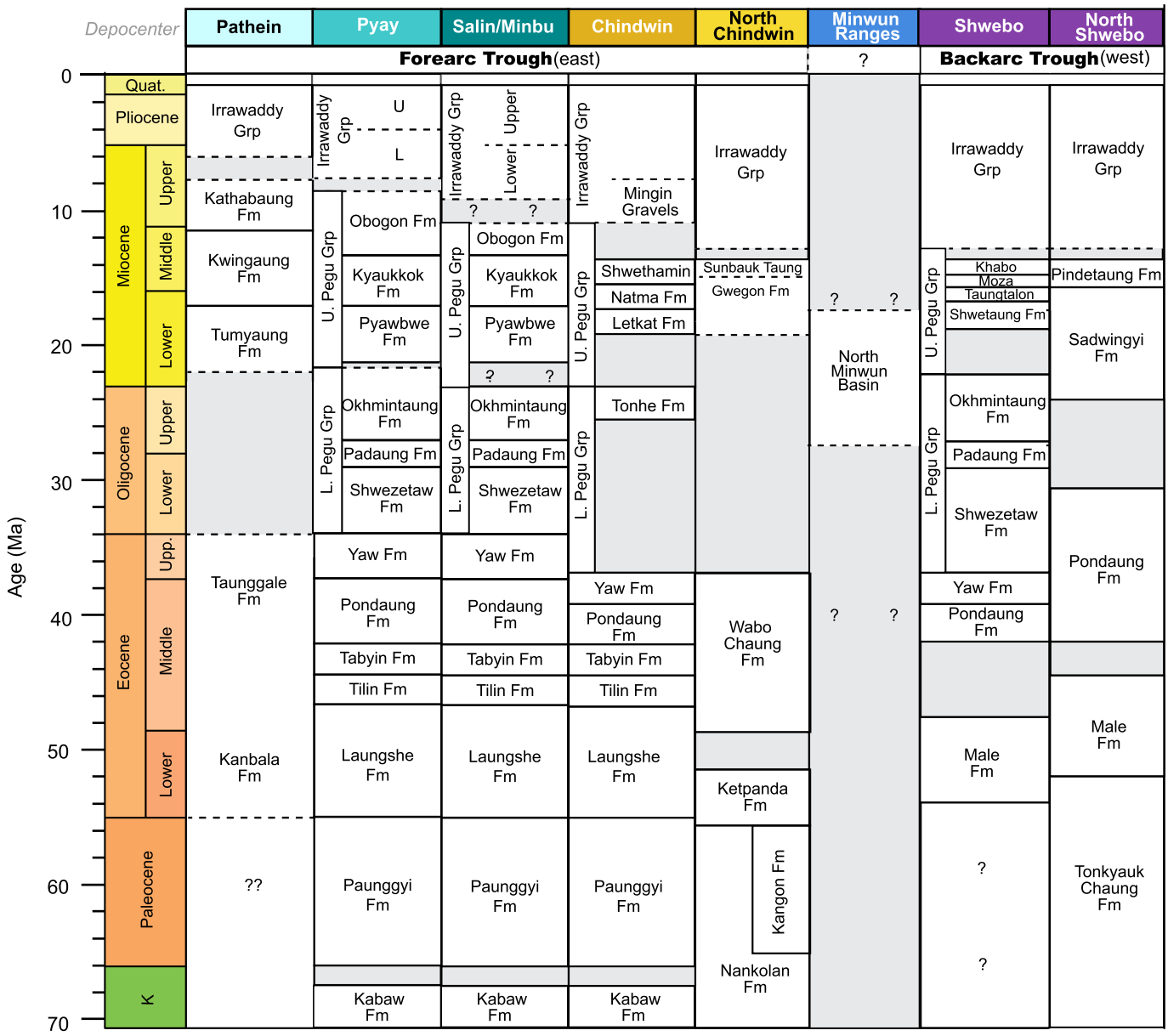

Fig. 2. Synthetic log of Upper Cretaceous-Quaternary Central Myanmar Basin (CMB) stratigraphy, major subbasins and depocenters, and key fluvio-deltaic sectors used for this study. Sectors are in reference to modern geography to orient reader. Stratigraphy modified after Arboit et al. (2021); Bender (1983); Khin and Myitta, 1999; Licht et al., 2018; Robinson et al., 2014; Thein and Maung, 2017; Westerweel et al., 2020; Zhang et al., 2019). Northernmost basins, the Hukawng and Putao basins (Fig. 1C), are without provenance data and so not considered here.

4.2. Zircon U–Pb geochronology

Nine samples for zircon U–Pb geochronology were prepared using standard heavy mineral separation methods at Birkbeck College, London. Strongly magnetic material was removed using a rare-earth-element magnet prior to sieving to 63–250 µm. Zircon grains were mounted in epoxy, polished, and imaged before analysis. U–Th–Pb isotopic compositions were determined at the London Geochronology Centre at University College London with a New Wave 193 nm aperture-imaged frequency-quintupled laser ablation system, coupled to an Agilent 7700 quadrupole-based ICP-MS. Full analytical details, including age standard and data reduction methods, are in the Supplementary Information. Individual U–Pb ages are reported at 1σ in Table S5. For grains with ages $\leq$1200 Ma, the $^{206}Pb/^{238}U$ ratio was used, and the $^{207}Pb/^{206}Pb$ ratio for grains $\geq$1200 Ma. Grain ages were filtered using a +5 and −20% discordance cut-off for ages $\geq$500 Ma.

Table S6 presents compiled zircon U–Pb datasets for CMB and source bedrock. To facilitate and normalize comparisons, raw U–Pb ages from the available literature were re-filtered using the same age and U–Pb discordance cutoffs. Zircon U–Pb results are presented as pie diagrams and kernel density estimates (KDE) for visual comparison. Quantitative comparison by multidimensional scaling (MDS) used the R 'provenance' package (Vermeesch et al., 2016). MDS, which is a form of PCA, takes high-dimensional distributional data compared by a statistical measure of similarity and reprojects results into reduced dimensions (i.e., biplot) for visualization.

4.3. Sr and Nd isotope geochemistry

Eleven delta samples were separated into <2 µm and >2 µm fractions and analyzed for Sr and Nd isotope geochemistry at GEOMAR Helmholtz Centre for Ocean Research Kiel (Table S3;

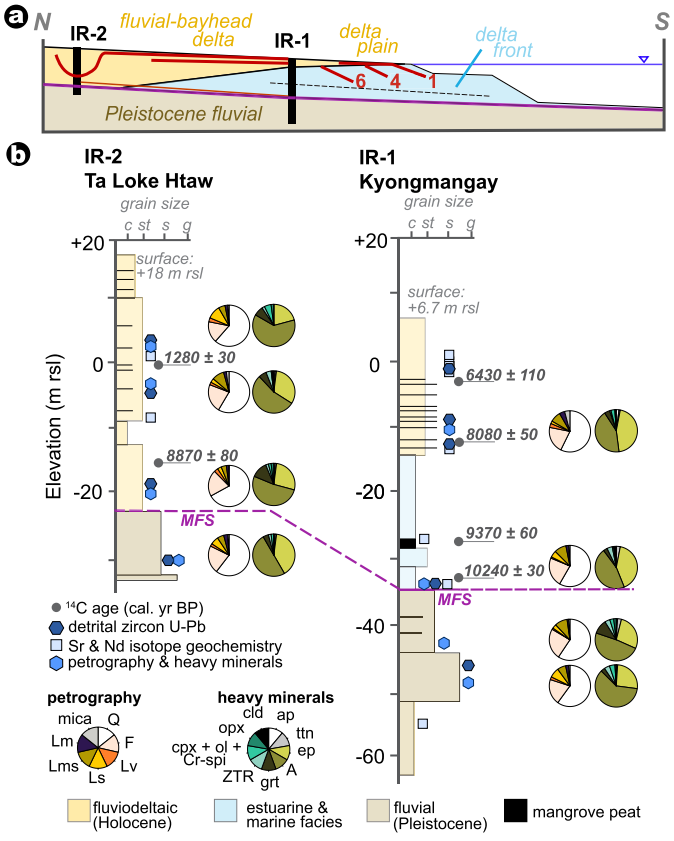

Fig. 3. Pleistocene-Holocene Irrawaddy Delta core lithostratigraphy and chronology. (A) Schematic section and inferred evolution of Irrawaddy Delta stratigraphy after Giosan et al. (2018). Red lines indicate location and age (in kyr) of delta front. (B) New petrographic and heavy mineral results alongside core lithostratigraphy and ages. Detailed sampling information and results in Tables S1–S3. Abbreviations: A–amphibole; ap–apatite; c–clay; cld–chloritoid; cpx–clinopyroxene; Cr-spi–Cr-spinel; ep–epidote; F–feldspars; grt–garnet; L-lithic fragments (Ls–sedimentary; Lm–medium-to high-rank metamorphic; Lms–low-rank metasedimentary; Lv–volcanic + metavolcanic); mica–biotite + muscovite; MFS–maximum flooding surface; ol–olivine; opx–orthopyroxene; Q–quartz; s–sand; st–silt; ttn–titanite (sphene); ZTR–zircon + tourmaline + rutile.

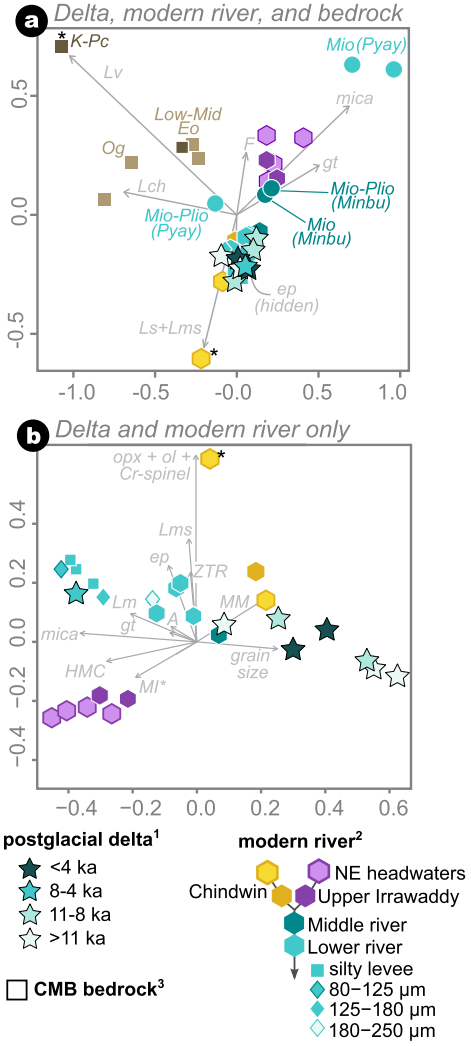

Fig. 4. Multivariate analysis of petrographic and heavy mineral data from the Irrawaddy Delta, River, and regional bedrock. (A) PCA of delta, river, and published CMB sedimentary bedrock show that modern river and postglacial delta sediments are distinct from older CMB bedrock; (B) PCA of postglacial delta and modern river only. Sample compositions are represented as points where petrographic or heavy minerals phases and indices are shown as rays. Ray length is proportional to the variance of the variable (i.e., mineral phase or index) among samples. If angle is close to 0°, 90°, 180°, variables are directly correlated, unrelated, or inversely correlated, respectively. Asterisks designate outliers far beyond axes. Median grain diameter is used as a grain size proxy (Table S2). Abbreviations: A–amphibole; ep–epidote; F–feldspar; grt–garnet; HMC–Heavy Mineral Concentration index; L = lithic fragments (Lch–chert; Lms–low-rank metasedimentary; Lm–high-rank metamorphic; Ls–sedimentary; Lv–volcanic); MI*–Metamorphic Index; mica–biotite + muscovite; MM–metamorphic minerals; ol–olivine; opx–orthopyroxene; ZTR–sum of zircon, tourmaline and rutile over total transparent heavy minerals. Data: 1) delta (this study); 2) modern river (Garzanti et al., 2016); 3) CMB (Najman et al., 2020; Zhang et al., 2019).

Bretschneider et al., 2021). All samples were pre-treated to remove authigenic Fe-Mn oxyhydroxides, fully decarbonated with 40% acetic acid, and finally separated and purified following standard ion chromatographic procedures. Sr isotope measurements were performed on a Nu Plasma high-resolution multi collector-inductively coupled plasma-mass spectrometer (MC-ICP-MS), while Nd isotope analyses were carried out on a Thermo Scientific Neptune Plus MC-ICP-MS at GEOMAR. Analytical details are in the Supplementary Information, with new and compiled Sr and Nd isotope data in Table S4.

5. Results and interpretations

5.1. Petrography and heavy minerals

Upper Pleistocene-Holocene fluviodeltaic sediments are similar to modern Irrawaddy river sands and levee silts, modern sands at Bagan (middle trunk river) and the Chindwin River tributary (Fig. 4). Sands are mostly litho-feldspatho-quartzose, with plagioclase ≈ K-feldspar. Sedimentary to very-low-rank metasedimentary rock fragments prevail over higher-rank metamorphic and volcanic grains, and biotite prevails over muscovite. Moderately-rich transparent heavy mineral assemblages are dominated by hornblende and epidote, with minor garnet, actinolite, and clinopyroxene. Miocene to Mio-Pliocene units display distinct signatures from Quaternary samples (Fig. 5). Relative enrichment of more stable heavy mineral phases (zircon, rutile, tourmaline, spinel, and apatite) with time indicates that the observed mineralogical variability (Table S3) is partly controlled by selective dissolution during diagenesis. Epidote, scarce garnet, chloritoid, mica, and total feldspar, however, show no age trend and are richest in Miocene bedrock. Paleogene and Eocene formations are characterized by very abundant plagioclase and mafic volcanic fragments.

Grain size controls petrographic and mineralogical signatures in postglacial fluviodeltaic sediments (Fig. 4A), as observed for Irrawaddy silt and sand (Garzanti et al. (2016). Mica is strongly anticorrelated with grain size. Lower Irrawaddy silty sands and mid-Holocene silts are richer in metamorphic lithics and heavy

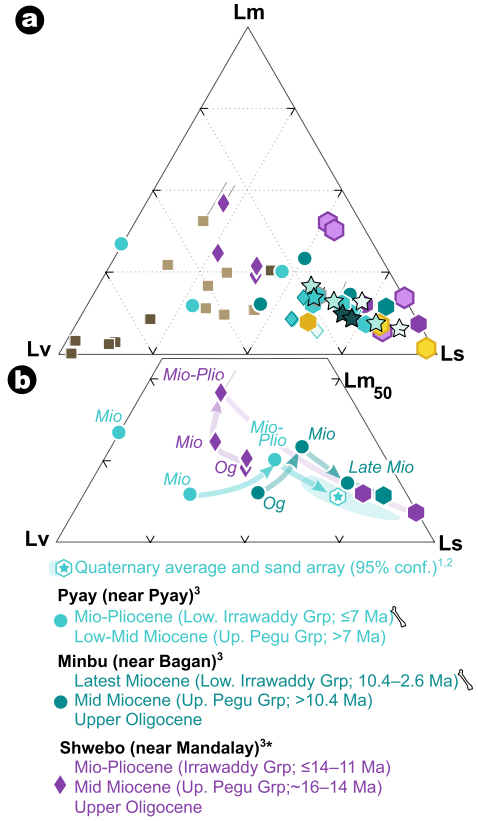

Fig. 5. (A) Lm-Lv-Ls ternary diagram, with (B) temporal evolution of the Pyay, Minbu, and Shwebo subbasins relative to the average Quaternary Irrawaddy. Light blue field represents 95% confidence ellipse around all coarse silt-sand Quaternary Irrawaddy samples. Pyay, Minbu, and Shwebo subbasins can be used as proxies for the past lower trunk Irrawaddy, middle trunk Irrawaddy, and lower Upper Irrawaddy signatures, respectively. L = lithic fragments (Lm = metamorphic; Lv = volcanic to low-rank metavolcanic and ultramafic; Ls = sedimentary to low-rank metasedimentary; Lch-chert). Symbols after Fig. 4. Bone icons indicate rock units with biostratigraphic and magnetostratigraphic age constraints (Section 6.1). Data: 1) delta (this study); 2) modern river (Garzanti et al., 2016); 3) CMB subbasins (Najman et al., 2020; Zhang et al., 2019). Asterisk denotes samples from subsurface.

minerals (especially garnet and amphibole) than coarser delta sediments. Diagenesis and hydraulic sorting are not the sole drivers of compositional variability between the modern lower and middle trunk, and their putative Miocene and Mio-Pliocene equivalents from the Minbu and Pyay subbasins. All Quaternary sediments, regardless of grain size, plot in PCA away from Miocene to Pliocene units that cluster near the modern Upper Irrawaddy and NE headwaters. Evidence against complete diagenetic and hydraulic control is illustrated by clustering of Chindwin River samples with the lower river and postglacial samples, and by K-feldspar and garnet enrichment in Miocene and Mio-Pliocene bedrock. In the Minbu subbasin, low-rank to high-rank metamorphic lithic fragments increase up-section into the mid-late Miocene (>10.4 Ma; Fig. 5A). The Pyay subbasin by the Mio-Pliocene (≤7 Ma) records a broadly similar trend toward compositions typical of the mid-late Miocene Minbu subbasin. Only by the late Miocene do total sedimentary fragments increase in the Pyay and Shwebo subbasins, where both become comparable to modern river equivalents.

5.2. Sr and Nd isotope geochemistry

Overall, Quaternary Irrawaddy sediments display an array of compositions where $^{87}Sr/^{86}Sr$ and ε_{Nd} values broadly decrease with grain size (Fig. 6A). $^{87}Sr/^{86}Sr$ values for clay (<2 μm) range between 0.714587 and 0.717801 (±0.000034, 2σ; average = 0.716520 ± 0.00097) with ε_{Nd} values of −6.9 to −5.8 (±0.1, 2σ; average = −6.5 ± 0.6). Silt and sand (>2 μm) show slightly less radiogenic $^{87}Sr/^{86}Sr$ (0.711579–0.716625; average = 0.71430 ± 0.00258) and less radiogenic ε_{Nd} values (−9.0 to −7.9; average = −8.6 ± 0.5). Quaternary Irrawaddy sediments (especially the <2 μm fraction) are overall more radiogenic than previously recognized for the modern lower river (ε_{Nd} − 10.7 to −8.1; Allen et al., 2008; Colin et al., 1999; Licht et al., 2016; Zhang et al., 2019). No coherent temporal trends are observed within the postglacial delta.

CMB sedimentary bedrock compositions broadly evolve toward less radiogenic ε_{Nd} values and more radiogenic $^{87}Sr/^{86}Sr$ values through time. The longest and most thorough record for ε_{Nd} values exists in the Minbu subbasin. The Lower Irrawaddy Group fine fractions document a significant shift (3–5 ε_{Nd} units) to some of the least radiogenic values in the late Miocene. By deposition of the Plio-Pleistocene Upper Irrawaddy Group, fine fractions return to more radiogenic values and remain through the Quaternary. Coarser sediment indicates a similar if smaller perturbation (≤3.5 ε_{Nd} units) by the late Miocene and clearly by deposition of the Upper Irrawaddy Group where ε_{Nd} decreases again by 0.5–6.1 units into the Mio-Pliocene. After which time, ε_{Nd} gently increases into the Quaternary. Modern Irrawaddy ε_{Nd} values are broadly consistent with Quaternary values, although the coarsest samples appear biased to more negative values in both size fractions.

Few $^{87}Sr/^{86}Sr$ data exist for the Mio-Pliocene Irrawaddy basin. Along with one late Miocene sample from the Minbu subbasin, two analyzed samples from the Yangon and Sittaung rivers can offer insight into Mio-Pliocene Sr–Nd signatures. These rivers primarily erode Upper Miocene to Lowermost Pliocene strata deposited within the lower Irrawaddy sector and so may be suitable compositional proxies for the lower Irrawaddy (Fig. 1). These data indicate a shift to more radiogenic $^{87}Sr/^{86}Sr$ synchronous with less radiogenic ε_{Nd} values (Fig. 6B and C).

Hydraulic sorting is well known to systematically decouple silt and clay isotopic signatures (Garçon et al., 2013). Among rivers draining average Upper Continental Crust ($\varepsilon_{Nd} = -10.4$), the difference between silt and clay ε_{Nd} values (termed $\Delta\varepsilon_{Nd}$) typically ranges between +1 and −1 (Bayon et al., 2015). Irrawaddy sediments document a larger offset ($\Delta\varepsilon_{Nd} \approx +2.1$) than the global river average. Greater decoupling can be observed in large river basins with lithological diversity and in those draining volcanic and/or volcaniclastic bedrock producing smectite and vermiculite clays. Volcanogenic clays tend to be overrepresented in the finer-grained suspended load, whereas crystalline detritus is overrepresented in coarser bedload (Bayon et al., 2015; Garçon et al., 2013). The Irrawaddy drainage exposes diverse lithologies in terms of Nd isotopes (Fig. 6), with an abundance of Cretaceous-Oligocene volcaniclastic (~58% drainage area) and Mesozoic ultramafic (~3%) bedrock which together may explain the decoupling between clay-silt and therefore high $\Delta\varepsilon_{Nd}$.

Isotopic, petrographic, and heavy mineral data suggest that coarse and very fine (<2 μm) Irrawaddy River sediment may sometimes record disparate provenance. Finest fractions appear to be primarily derived from ε_{Nd}-rich volcanic rocks and volcaniclastic strata, such as Upper Cretaceous to Eocene formations of the CMB and IBR. Crystalline bedrock exposed along the MMB, DB, and Gaoligong Shear Zone yield radiogenic $^{87}Sr/^{86}Sr$ values, quartz, K-feldspar, and an array of heavy minerals that concentrate in coarser silts and sands.

5.3. Zircon U–Pb geochronology

Zircon U–Pb ages in Upper Pleistocene-Holocene fluviodeltaic sediments range from Miocene to late Archean, with 23–43% of ages between 15–80 Ma, 16–25% between 80–130 Ma, with variable subordinate clusters at ~400–600 Ma, ~850–1200 Ma, and

Fig. 6. (A) $^{87}Sr/^{86}Sr$ and ε_{Nd} crossplot for the Irrawaddy Basin, including bedrock sources and neighboring rivers. Plots of ε_{Nd} for the CMB subbasins through time: (B) silt-sand fraction (C) clay fraction. Corresponding $^{87}Sr/^{86}Sr$ results are not available for all ε_{Nd} data shown in (B) and (C). Published data: <2 μm, clay, fine silt, and bulk mud samples shown as circles; >2 μm, >63 μm, sand, and bulk sediments without grain size information shown as squares. Data: 1) this study; 2) Bretschneider et al., 2021; 3) Colin et al., 1999; 4) Allen et al., 2008; 5) Giosan et al., 2018; 6) Zhang et al., 2019; 7) Damodararao et al., 2016; 8) see Supplementary Information; 9) Licht et al., 2013; 10) Licht et al., 2016.

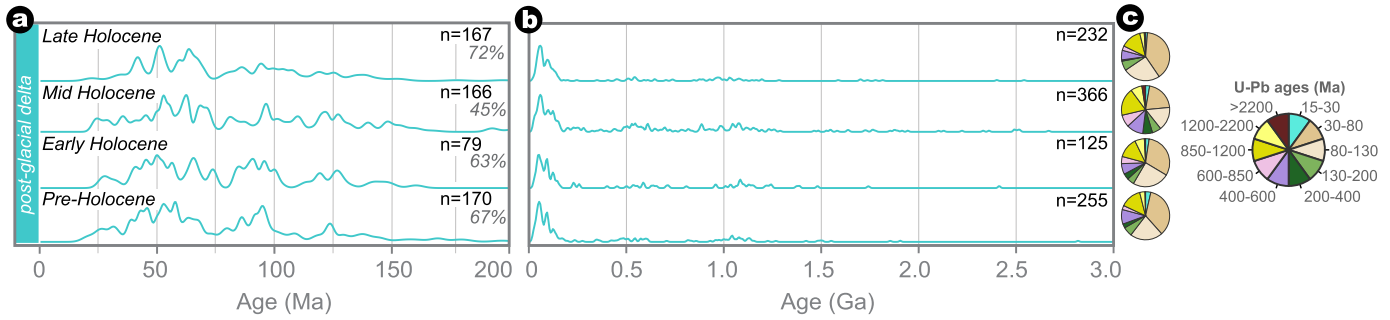

Fig. 7. Kernel density estimate (KDE) plots showing postglacial Irrawaddy delta detrital zircon U–Pb ages from (A) 0–200 Ma (number and percentage of ≤200 Ma grains are indicated) and (B) 0–3000 Ma. Data in Table S5.

1200–2200 Ma (Fig. 7). Mid-Holocene sediment features slightly older zircon populations (>200 Ma; 55%) and more common Permo-Triassic ages (200–400 Ma; 7%). Pre-Cenozoic grains in the Irrawaddy Basin tend to be small and were noted to occur more frequently in fine-grained Irrawaddy samples from the lower reaches (Fig. 8; Garzanti et al., 2016). Pre-Cenozoic U–Pb ages are thus overrepresented in fine-grained sands of the mid-Holocene delta (Fig. 7). Coarse Upper Pleistocene-Holocene samples yield more young U–Pb ages (63–72% <200 Ma).

MDS analysis is consistent with derivation of modern Chindwin detrital zircon from mid-Eocene formations exposed in the CMB and IBR, as well as from Eo-Oligocene formations in the northern IBR and Naga Hills (Figs. 1, 8 and 9). Modern Upper Irrawaddy tributaries yield zircon populations like that of Oligocene IBR and Cretaceous-Eocene CMB bedrock, which may reflect similar bedrock terrane sources. Sands in modern NE headwaters (the Nmai and Mali Hka), instead, yield detrital zircon ages most akin to those of MMB, eastern DB and Sodon granitoids.

By the late Oligocene, the Shwebo subbasin and Minwun Ranges indicate increasingly young U–Pb zircon ages (<30 Ma) pointing at MMB and DB sources. To a lesser extent, this is also observed in the Chindwin subbasin that also includes abundant older Paleozoic and Precambrian zircon. Supply of MMB and DB granitoids remained steady throughout the Lower-Middle Miocene (~19–16 Ma) Letkat Formation in the Chindwin subbasin and the Lower-Middle Miocene Shwetaung Formation in the Shwebo subbasin. By deposition of the Upper Pegu Group (~16–14 Ma), the Shwebo subbasin increased in <30 Ma and 60–50 Ma ages derived, respectively, from MMB and DB plutons exposed near Mogok. The Gwegon Formation of the northern Chindwin subbasin records a similar spike in 80–30 Ma ages. Within the Pyay subbasin, both the middle Miocene Obogon Formation (~14–10 Ma) and Upper Miocene-Pliocene (≤7 Ma) Lower Irrawaddy Group show provenance distinct from the modern river. These units, like those of similar age in the Shwebo and Chindwin subbasins, show increased <30 Ma and 60–50 Ma zircon. Only after the Mio-Pliocene does the Shwebo subbasin, and indeed Pyay subbasin, evolve toward modern signatures.

6. Birth of the modern Irrawaddy

Many studies have investigated the history of the Irrawaddy drainage in terms of early Cenozoic magmatism and tectonism (Arboit et al., 2021; Licht et al., 2018, 2013, 2016; Robinson et al., 2014; Wang et al., 2014; Westerweel et al., 2020; Zhang et al., 2019). Three provenance shifts are broadly recognized in the CMB with onset of an ancestral Irrawaddy drainage: (1) an active and eroding Wuntha-Popa Arc, with increased recycling of Mesozoic and Paleozoic basement terranes in the latest Eocene-Oligocene; (2) increasing contribution of MMB detritus through the Oligo-Miocene, with reduction in Wuntha-Popa Arc activity after 32 Ma; and (3) increased erosional flux from the northern MMB region, including DB and the Gaoligong Shear Zone, into at least the middle Miocene. Rapid exhumation and cooling of the central MMB initiated by the late Oligocene (25–17 Ma) and progressed northward to Mogok and into DB by the early-mid Miocene (20–16 Ma; Bertrand et al., 2001; Socquet and Pubellier, 2005). Gaoligong Shear Zone shearing and exhumation initiated by ~23 Ma and continued to ~11 Ma, as constrained by zircon U–Pb and mica $^{40}Ar/^{39}Ar$ ages (Zhang et al., 2012). Apatite fission-track cooling ages mark the end of shearing in the southern Gaoligong Shear Zone by ~8.5 Ma, when left-lateral strike-slip motion in the west DB began (Wang et al., 2008). CMB sediments track the tectonic evolution of upstream sources through the mid-Miocene, with increased supply from metamorphic and granitoid rocks, increasingly negative ε_{Nd}, higher $^{87}Sr/^{86}Sr$, and greater proportions of ~25–20 Ma and 60–50 Ma detrital zircon U–Pb ages.

When was the onset of the modern Irrawaddy drainage? If we consider the 'birth' of the modern river as the time at which the river, including its major tributaries, achieved a geometry and provenance akin to present, it was not before the close of the Miocene that the modern Irrawaddy was born. Indeed, all Quaternary sediment in the lower reaches and delta have consistently different compositions than mid-late Miocene signatures. Petrographic, heavy mineral, and zircon results imply that modern-day compositions in the trunk Irrawaddy and Chindwin and Upper Irrawaddy tributaries were not attained until at least the latest Miocene. Nd isotopes might suggest an earlier mid-late Miocene onset, where signatures converge to near-modern values by deposition of the Upper Pegu Group Obogon Formation (~14–10 Ma; Fig. 6). In this scenario, the Irrawaddy Group signifies a short compositional perturbation after mid-late Miocene drainage establishment. While a mid-late Miocene onset is plausible, the lack of paired Sr–Nd Miocene data and strong grain size control on bulk isotope signatures (Section 4.2) make an early onset less convincing. All other datasets indicate that a river resembling the modern Irrawaddy drainage was not attained until the late Miocene, if not by the Pliocene. Furthermore, compelling evidence exists for drainage reorganization into Irrawaddy Group deposition, as explored below. These findings contrast with the popular notion that Irrawaddy River provenance remained stable after the middle Miocene (cf., Licht et al., 2016; Najman et al., 2020; Zhang et al., 2019).

We argue that an evolving Irrawaddy River provenance after the mid-late Miocene is in better agreement with kinematic reorganization of the Indo-Burman boundary into a hyper-oblique setting marked by development of a localized Sagaing Fault zone, followed by widespread inversion of the CMB. While provenance evolution after the mid-Miocene partly reflects waning exhumation of the northern MMB and DB, additional controls on sedimentary evolution are required to explain modern-day compositions of the trunk river and tributaries.

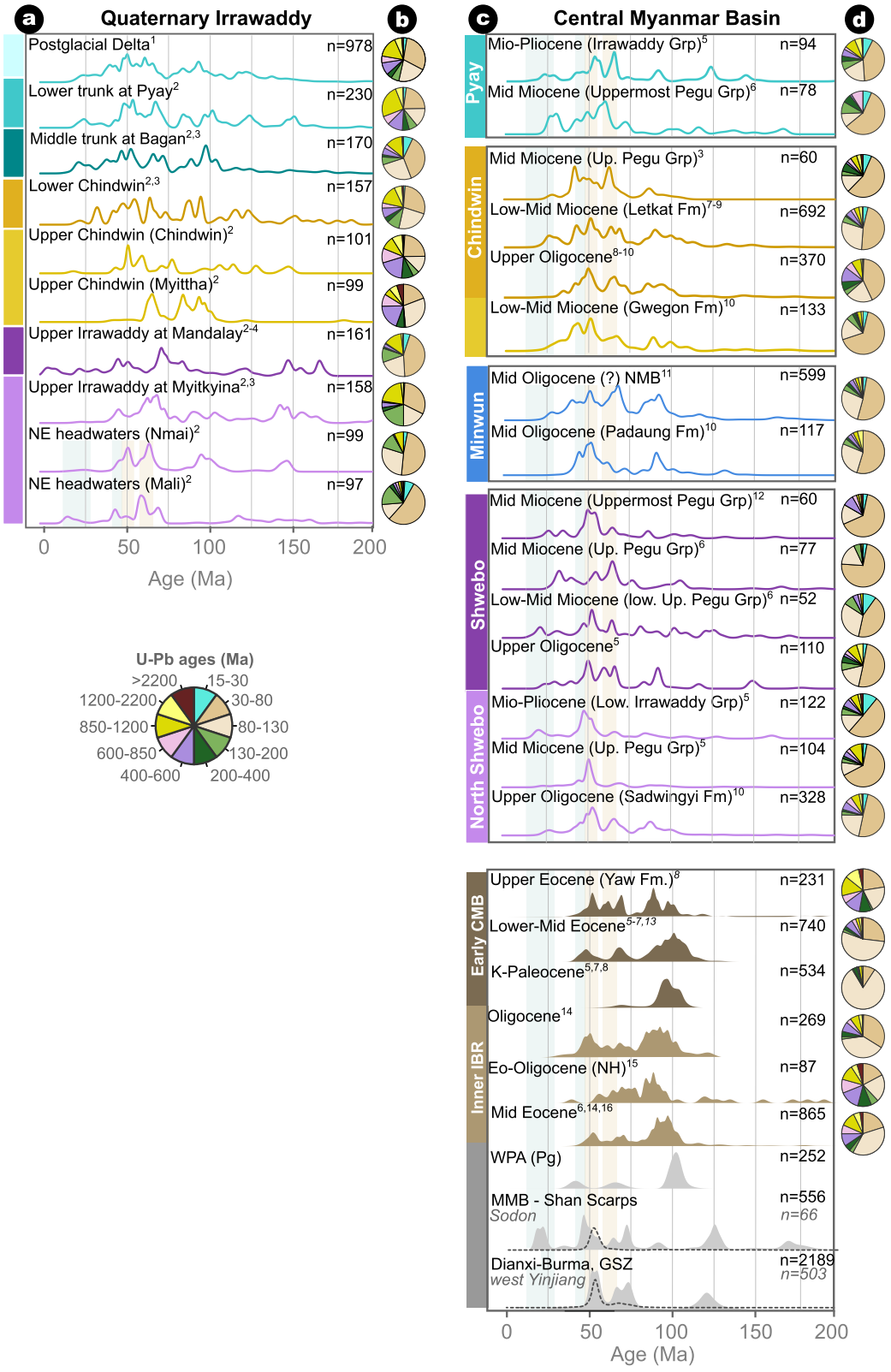

Fig. 8. (A–D) Composite kernel density estimate (KDE) plots and pies showing zircon U–Pb ages from 0–200 for the Quaternary river, CMB bedrock and selected source terranes. Datasets: 1) this study; 2) Garzanti et al., 2016; 3) Tang, 2013; 4) Bodet and Schärer, 2000; 5) Zhang et al., 2019; 6) Robinson et al., 2014; 7) Wang et al., 2014; 8) Licht et al., 2018; 9) Westerweel et al., 2020; 10) Arboit et al., 2021; 11) Morley and Arboit, 2019; 12) Liang et al., 2008; 13) Oo et al., 2015; 14) Naing et al., 2014; 15) Aitchison et al., 2019; 16) Najman et al., 2020. See Tables S5–S6 for full datasets.

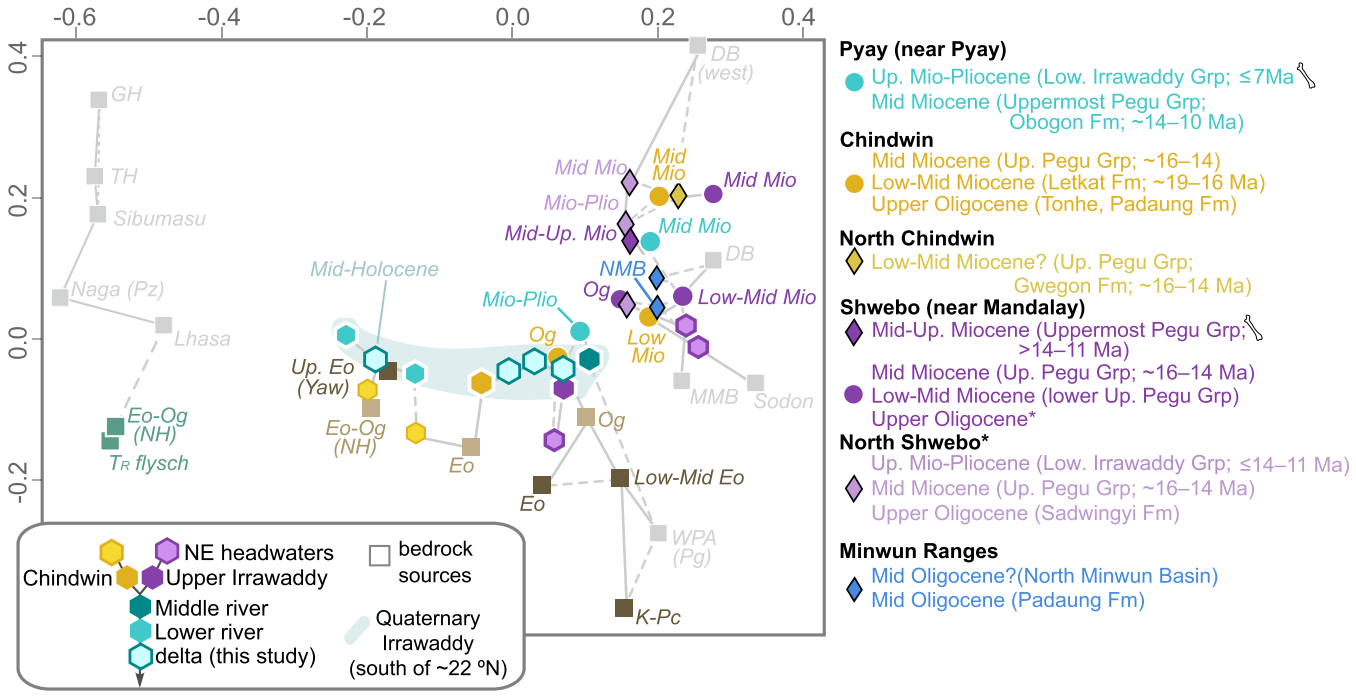

Fig. 9. Multidimensional scaling (MDS) plot using Kolmogorov-Smirnov dissimilarities for zircon U–Pb ages from the delta, modern river, and bedrock terranes. Diamonds indicate Miocene samples in Mu River catchment and Minwun Ranges. MDS utilizes pair-wise similarities between detrital zircon age distributions and reduces data into a 2D plot showing the degree of dissimilarity between samples as the distance between points. Solid gray lines indicate nearest similar neighbor; dashed gray lines second nearest neighbor. Stress = 6.327386. A goodness-of-fit or stress, less than 10% is considered 'good' for moderate to large datasets (Vermeesch et al., 2016). Gray field shows the compositional array of the modern lower Irrawaddy River. Bone icons indicate rock units with independent age constraints (Section 6.1). See Fig. 2 for CMB stratigraphy. Abbreviations: DB–Dianxi-Burma; GH–Greater Himalaya; GSZ–Gaoligong Shear Zone; NH–Naga Hills; NMB–North Minwun Basin; TH–Tethyan Himalaya. Data same as Fig. 8 and presented in Tables S5–S6.

6.1. CMB inversion and sediment recycling

Abundant stratigraphic, structural and seismic evidence documents CMB inversion initiated by the late Miocene (10 Ma) and peaked by the Plio-Pleistocene (Fig. 1C; Bender, 1983; Pivnik et al., 1998; Ridd and Racey, 2015; Sloan et al., 2017; Zhang et al., 2021). Inversion formed broad synclinoria within the Chindwin, Minbu, Pyay, and Shwebo subbasins. Inversion and erosion of 900–1200 m of section from the Bago Yoma anticlinorium alone is estimated (Ridd and Racey, 2015). East-verging thrust sheets, inferred to be active by the Plio-Pleistocene, presently demarcate the Chindwin and Mu River drainage divide (Fig. 1B). Contemporaneous thrust faults and en-echelon folds in the Minbu and Pyay subbasins at Bagan and Pyay, respectively, are incised by the modern river. Offshore records show rapid delta progradation and accumulation of ~4 km of sediment in the Gulf of Mottama from the mid-Miocene to Pleistocene (Khin and Myitta, 1999; Sloan et al., 2017).

Inversion-related drainage evolution is documented by the fluviatile Irrawaddy Group (Fig. 2), spanning from the mid-late Miocene and earliest Pliocene (Lower Irrawaddy Group) to the Plio-Pleistocene (Upper Irrawaddy Group). The base of the Irrawaddy Group is diachronous; its age decreases southward following southward progradation of the Irrawaddy River. In the northern Minbu subbasin, the Yenangyaung faunal assemblage ~30 km north of Magway suggests that the basal Irrawaddy Group is no older than 10–9 Ma (i.e., Takai et al., 2018). Magnetostratigraphy and mammalian fossils, including the hominoid *K. ayeyarwadyensis*, further support the basal Irrawaddy Group being no older than 10.4–8.8 Ma near Magway (Jaeger et al., 2011). A maximum age of ~7–6 Ma is inferred for the basal Irrawaddy Group farther south in the Pyay subbasin, based on upstream chronologies and the average progradation rate (Khin and Myitta, 1999; Takai et al., 2018). No maximum depositional ages are available for the Upper Irrawaddy Group, but the Gwebin faunal assemblage near Bagan in the Minbu subbasin is Plio-Pleistocene (~2.6 Ma; Takai et al., 2018). Upper Irrawaddy Group strata analyzed for Sr and Nd isotope geochemistry (Fig. 6) by Licht et al. (2013) are ≤3 km from the Gwebin locality.

Late stages of inversion drove widespread recycling of old CMB material to the offshore and entrenchment into floodplains. This is evidenced by incision of inversion-related structures in the western trough (Fig. 1B) and polycyclic sediment. Pyay subbasin detrital zircon signatures evolved after the mid-late Miocene (~14–10 Ma) to a provenance similar to Eo-Oligocene sedimentary bedrock (Fig. 9). Recycling of Eo-Oligocene bedrock zircon becomes especially clear by deposition of the Mio-Pliocene Irrawaddy Group (≤7 Ma) at Pyay. Entrenchment is similarly documented by lithic fragment evolution (Fig. 5), with recycling initiating after deposition of the Upper Pegu Group. By deposition of the Lower Irrawaddy Group (≤7 Ma) at Pyay, lithic fragments had evolved directly toward compositions like the Upper Pegu Group incised upstream near Bagan (Fig. 5B). Isotope geochemistry trends are less clear but all size fractions reach modern-day compositions by latest Pleistocene.

6.2. Beheading of the Chindwin and Mu Rivers

The two main Irrawaddy tributaries, the Chindwin and Upper Irrawaddy, are compositionally distinct and reflect either a recycled CMB and volcaniclastic IBR provenance or a mixed metamorphic belt-granitoid provenance, respectively. It is well-recognized that as early as the Oligocene and until the mid-late Miocene, the Chindwin subbasin received significant metamorphic input from MMB and DB sources based on lithic fragments, detrital minerals, and mineral geochemistry (Arboit et al., 2021; Licht et al., 2018, 2016; Morley and Arboit, 2019; Westerweel et al., 2020; Zhang

et al., 2019). Miocene signatures are at odds with what is observed today. The modern Chindwin drains no part of the MMB, DB, or Gaoligong Shear Zone (Fig. 1). The simple observation that the modern drainage cannot reproduce Miocene signatures necessitates drainage reorganization, characterized by a loss of key headwaters once yielding MMB and DB detritus (Fig. 10).

Drainage reorganization initiated as early as 14 Ma and certainly after 7 Ma. Pinpointing a more precise interval is difficult for several reasons. To-date, there are few/no provenance data on strata younger than the Lower-Middle Miocene for the Chindwin subbasin. Secondly, many Neogene-Quaternary CMB formations are polycyclic, whereby younger formations partially rework older formations. This polycyclicity provides further evidence for significant basin inversion as described above (Section 5.1). Establishing absolute ages for Neogene-Quaternary formations is difficult, partly because extensive recycling prevents obtaining true depositional ages and yields only older maximum depositional ages (Arboit et al., 2021; Westerweel et al., 2020; Zhang et al., 2019). Biostratigraphic and magnetostratigraphic chronologies are rarely available at the same locations as detrital geo- and thermochronological samples. Identifying a clear cessation for MMB and DB detritus is also practically impossible. Even after cessation of metamorphic supply, older MMB and DB detritus could be reworked, albeit in possibly reducing quantities through time. Despite these challenges, we summarize the data in context to regional stratigraphy (Fig. 2) to constrain timing of drainage reorganization.

An absolute maximum age limit is confidently estimated from the fluviatile Lower-Middle Miocene Letkat Formation (~19–16 Ma). Metamorphic detritus in the Chindwin subbasin is documented by the late Oligocene (27 Ma; Arboit et al., 2021; Morley and Arboit, 2019) and up to deposition of the Letkat Formation. Youngest detrital apatite fission track ages range from ~19–17 Ma, with one youngest U–Pb detrital zircon age of 16.8 ± 1.3 Ma from the top of the Letkat Formation (Licht et al., 2018; Wang et al., 2014; Westerweel et al., 2020). Mammalian fauna from overlying Irrawaddy Group Mingin Gravels were assigned to the mid-late Miocene (14–11 Ma; Bender, 1983; Takai et al., 2018), constraining the Letkat Formation is no younger than mid-Miocene. An early-mid Miocene age (19–16 Ma) can thus be confidently assigned to the Letkat Formation. This places a maximum age for headwater reorganization, as the Chindwin clearly received MMB and DB input until that time.

A second upper age limit can be inferred from the Upper Pegu Group now encompassed within the modern Mu River catchment (Fig. 1A). Strata show input from the MMB and DB until at least the mid-late Miocene (Fig. 9). The modern Mu River erodes neither of these sources today so likewise requires drainage reorganization to explain provenance and geometry. First, MDS analysis groups together the Upper Pegu Group and Gwegon Formation. Although considered a time-stratigraphic equivalent to the Letkat Formation (Arboit et al., 2021), MDS suggests that the Gwegon Formation shares much closer similarity to the Upper Pegu Group in the Chindwin subbasin (Tang, 2013), at Mandalay, and in the north Shwebo subbasin (Robinson et al., 2014; Zhang et al., 2019). The Upper Pegu Group is stratigraphically younger than the Letkat Formation but older than basal Irrawaddy Group containing mid-late Miocene (~14–11 Ma) fauna (Bender, 1983; Takai et al., 2018). If a mid-Miocene (~16–14 Ma) age is assigned to the Upper Pegu Group and Gwegon Formation in the modern Mu catchment, then beheading of Shwebo and Chindwin subbasin headwaters occurred no earlier than 16–14 Ma.

The uppermost Upper Pegu and Lower Irrawaddy groups belong to a second MDS cluster. The Lower Irrawaddy Group is no older than ~14–11 Ma in the eastern trough, which places limits on the underlying uppermost Upper Pegu Group at Mandalay. The Lower Irrawaddy Group in the Pyay subbasin further constrains

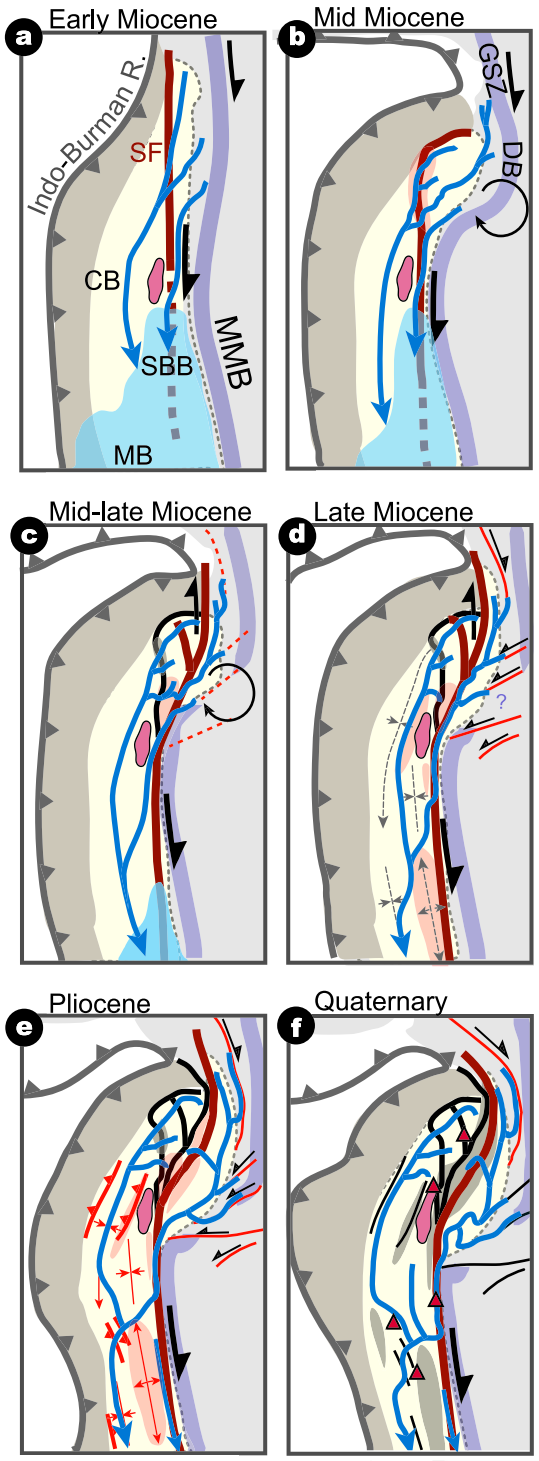

Fig. 10. Schematic evolution of the Irrawaddy drainage following Miocene tectonic reorganization of Southeast Asia, adapted from Morley and Arboit (2019). By the early Miocene (A), exhumation of the MMB and movement along the Gaoligong Shear Zone (GSZ) are well underway. Metamorphic and granitoid detritus fed to the ancestral rivers of the Central Myanmar Basin. (B) India-Asia collision drives extrusion of SE Asia, accommodated by Sagaing Fault movement, GSZ shearing, and clockwise rotation of Dianxi-Burma (DB). Rivers erode back into the metamorphic highlands and exhumation continues. (C) Curving disrupts Western Sagaing Fault movement and activates straighter, eastward splays through time. Sinistral faults in Dianxi-Burma activate and terminate the GSZ. (D) Topographic uplift among Sagaing Fault splays drives capture of western Chindwin Basin (CB) headwaters and expansion of Upper Irrawaddy tributary. (E) and (F) CMB inversion ramps up into the Plio-Pleistocene. The nascent Irrawaddy River is pinned into place. Thrust sheets and tectonic ridges along eastern Sagaing Fault strand fully isolate the Mu River catchment.

the uppermost Upper Pegu Group at Pyay to be mid-late Miocene (~14–10 Ma). All units indicate metamorphic detritus supply. Metamorphic rock fragments increase through the mid-Miocene, and only after deposition of the Lower Irrawaddy Group do high-rank metamorphic fragments rapidly decrease (Fig. 5). While waning exhumation in the MMB and DB surely influences provenance signatures, the distinct lack of modern headwaters eroding key MMB and DB sources still mandate headwater drainage capture after 11 Ma.

6.2.1. Role of the Sagaing Fault

We further evaluate drainage capture and formation of distinctive Chindwin, Upper Irrawaddy, and Mu river catchments using evidence from the synkinematic North Minwun Basin (NMB) and the Sagaing Fault. Today, the NMB is part of the Minwun Ranges that stretch from ~25° to 23.5° N along the Sagaing Fault and altogether form the central drainage divides among the modern Chindwin, Upper Irrawaddy, and Mu rivers. The NMB yields a robust mid-Oligocene maximum depositional age at ~28–27 Ma from detrital zircon, rutile and apatite (Morley and Arboit, 2019). Youngest detrital zircon yield a mean-weighted U–Pb age of 23.4 ± 0.5 Ma and two apatite yield ages at 23.4 ± 5.5 Ma and 25.9 ± 2.0 Ma. MDS indicates statistical similarity among the NMB, Letkat Formation, Upper Oligocene bedrock, and the Upper Pegu Group of the Shwebo subbasin (Fig. 9). While an age as young as the Letkat Formation (~19–16 Ma) could be inferred for the NMB, Letkat Formation detrital zircon (16.8 Ma; Wang et al., 2014) and apatite (~22–20 Ma; Westerweel et al., 2020) remain consistently younger than even the youngest NMB grains. Therefore, while an Oligocene (~27 Ma) age is not explicitly precluded, provenance and youngest detrital U–Pb ages reassign the NMB to Oligo-Miocene.

If the NMB is Oligo-Miocene (~23 Ma), its synkinematic nature warrants that the West Sagaing Fault was active during this time. This initiation predates the last observed shift in CMB provenance by several million years. MMB and DB detritus supplied the Chindwin subbasin until at least ~14 Ma and ~11 Ma in the north Shwebo subbasin. After which, key headwaters were lost. We find it likely that sequential activation of eastern strands through the Miocene compounded with late Miocene inversion to reorganize headwaters. Cumulative deformation and dextral displacement on the Sagaing Fault aided rerouting of headwaters exclusively into the Upper Irrawaddy, whereafter protracted inversion further delineated modern catchments and drove wholesale entrenchment.

Abundant structural, stratigraphic, and provenance evidence for late Miocene inversion, existing near and far from the Sagaing Fault (i.e., Pivnik et al., 1998; Bender, 1983; this study), precludes Sagaing Fault deformation as the sole mechanism driving drainage reorganization. Yet strike-slip deformation has clearly influenced river morphology since at least the Quaternary, as demonstrated by the remarkably linear 180-km stretch of the Upper Irrawaddy along the Sagaing Fault and the trellised drainage among 'basin-and-range' topography of the northern horsetail splays (Soe Thura and Watkinson, 2017). Crucially, the eastern margins of the modern Chindwin and Mu catchments are defined by curvilinear ranges uplifted by the Sagaing Fault, including the Minwun Ranges. Data synthesized here place important constraints on topographic development along the Sagaing Fault. If drainage reorganization was related to Sagaing Fault deformation, topography was not significant enough to perturb Chindwin headwaters until after ~14 Ma and after 11 Ma in the northern Shwebo subbasin.

6.3. Tectonic summary

The modern Irrawaddy River is a product of deformation set in motion by a two-stage kinematic reorganization of the Indo-Burman margin during India-Asia collision. First, an earliest Miocene period of hyper-oblique convergence was characterized by north-south translation along an incipient Sagaing Fault and rapid clockwise rotation of crustal blocks around the Eastern Himalayan Syntaxis. Early to mid-Miocene mica cooling ages mark cessation of NW-SE to N-S shearing and initiation of rapid exhumation along the Shan Scarps and MMB by ~22–16 Ma (Bertrand and Rangin, 2003; Bertrand et al., 2001; Lamont et al., 2021; Socquet and Pubellier, 2005), roughly coeval with initiation of the West Sagaing Fault by ~23 Ma (Arboit et al., 2021; Morley and Arboit, 2019). Rivers expanded up into major shear zones to erode and transport metamorphic detritus through the CMB (Arboit et al., 2021; Zhang et al., 2019). Supply of metamorphic detritus to large fluviodeltaic and estuarine systems in the Chindwin, Minbu, and Shwebo subbasins is sustained until at least the middle (~14 Ma) to mid-late Miocene (~11 Ma).

Extrusion of crustal material out of and around the Eastern Himalayan Syntaxis provoked right-lateral shearing in the Gaoligong Shear Zone and differential, clockwise rotation of tectonic blocks in the DB and northern MMB regions. By the mid-Miocene, exhuming dextral shear zones transitioned into broad accommodation zones for left-lateral and transtensional faults (Socquet and Pubellier, 2005; Wang et al., 2008; Zhang et al., 2012). Elsewhere, clockwise rotation disrupted older established structures. Bending of the West Sagaing Fault led to activation of strands eastward through time (Morley and Arboit, 2019). Activation of the easternmost strand took place no earlier than 20–18 Ma, at least near Mogok (Lamont et al., 2021). Interaction among releasing and restraining bends generated topographic relief. Transpression, extensional duplexing, and/or detachment faulting are all suggested mechanisms generating curvilinear uplifts along the Sagaing Fault (i.e., Soe Thura and Watkinson, 2017). Headwaters routing from the metamorphic highlands to the Chindwin subbasin were beheaded only after ~14 Ma. North Shwebo subbasin headwaters, if not also those of the Chindwin, were lost after ~11 Ma. Reorganization at this time is broadly consistent with falling or rising sediment accumulation rates in west and east subbasins, respectively (Zhang et al., 2021).

By 10–8 Ma, India-Eurasia convergence decreased in obliquity and the tectonic regime in Myanmar shifted from transtension to transpression (Maurin and Rangin, 2009; Pivnik et al., 1998; Zhang et al., 2021). Regional inversion was the last impetus driving wholesale drainage reorganization of the modern Irrawaddy sediment-routing system. Folding pinned the nascent drainage into its characteristic bifurcate geometry, with only the Upper Irrawaddy tributary draining the metamorphic highlands. A shallow synclinorium formed the Mu River catchment, with east-verging thrusts sealing off the western drainage divide by the Plio-Pleistocene (Pivnik et al., 1998). Late Miocene to Pliocene entrenchment drove floodplain cannibalization onshore and rapid southward migration of major marine depocenters into the Gulf of Mottama (Khin and Myitta, 1999; Ridd and Racey, 2015). The Irrawaddy River converged toward a modern-day geometry and provenance by the latest Miocene. After the height of Pliocene-Pleistocene inversion (Pivnik et al., 1998), the drainage was locked into its present configuration following transfer of shortening into the IBR wedge after 2 Ma (Maurin and Rangin, 2009).

7. Conclusions

For the first time, a detailed Miocene-Recent provenance evolution for the Irrawaddy sediment-routing system is explored across key sectors of the drainage through space and time. Multi-method provenance analyses of the postglacial Irrawaddy delta, in combination with upstream Cenozoic bedrock datasets, help define an evolving river through the late Neogene. Deposition of the Irrawaddy Group marks not only a stark stratigraphic change across

the CMB but initiation of a last significant shift in provenance for the entire Irrawaddy Basin. A unique Quaternary Irrawaddy provenance is as of yet unrecognized, and contrasts with prevailing assumptions that Irrawaddy River provenance remained stable since the mid-Miocene. We reveal an evolving drainage through the late Neogene that is more compatible with tectonic reorganization across Southeast Asia at that time. Disparate mid-late Miocene and Quaternary provenance signatures require drainage reorganization, with significant loss of headwaters feeding the Chindwin subbasin after ∼14 Ma and the northern Shwebo subbasin after ∼11 Ma. CMB inversion (≤10 Ma) was the primary driver of late Miocene-Quaternary provenance evolution but Sagaing Fault deformation crucially rerouted headwaters exclusively into the Upper Irrawaddy. Entrenchment of the trunk Irrawaddy and Chindwin rivers promoted large-scale sediment reworking after ∼7 Ma. Enhanced late Miocene-Pleistocene Irrawaddy sediment flux drove rapid southward delta progradation and significant sediment accumulation offshore.

CRediT authorship contribution statement

Tara N. Jonell: Conceptualization, Data curation, Formal analysis, Methodology, Visualization, Writing – original draft, Writing – review & editing. **Liviu Giosan:** Funding acquisition, Resources, Writing – review & editing. **Peter D. Clift:** Funding acquisition, Resources, Writing – review & editing. **Andrew Carter:** Formal analysis, Writing – review & editing. **Lisa Bretschneider:** Formal analysis. **Ed C. Hathorne:** Formal analysis, Writing – review & editing. **Marta Barbarano:** Formal analysis. **Eduardo Garzanti:** Formal analysis, Writing – review & editing. **Giovanni Vezzoli:** Formal analysis. **Thet Naing:** Resources, Writing – review & editing.

Declaration of competing interest

The authors declare that they have no known competing financial interests or personal relationships that could have appeared to influence the work reported in this paper.

Acknowledgements

We thank Chris Morley and Yani Najman for thoughtful and constructive reviews. TNJ was supported in initial stages of this project by a Postdoctoral Research Fellowship at UQ and software support by LSU. LG thanks support from the Andrew W. Mellon Foundation via Woods Hole Oceanographic Institution. The Charles T. McCord chair at LSU funded coring and detrital zircon U–Pb geochronology essential to the study.

Appendix A. Supplementary material

Supplementary material related to this article can be found online at https://doi.org/10.1016/j.epsl.2022.117516.

References

Aitchison, J.C., Ao, A., Bhowmik, S., Clarke, G.L., Ireland, T.R., Kachovich, S., Lokho, K., Stojanovic, D., Roeder, T., Truscott, N., Zhen, Y., Zhou, R.J., 2019. Tectonic evolution of the Western Margin of the Burma microplate Based on New Fossil and radiometric age constraints. Tectonics 38, 1718–1741.

Allen, R., Najman, Y., Carter, A., Barfod, D., Bickle, M.J., Chapman, H.J., Garzanti, E., Vezzoli, G., Andò, S., Parrish, R.R., 2008. Provenance of the Tertiary sedimentary rocks of the Indo-Burman Ranges, Burma (Myanmar): Burman arc or Himalayan-derived? J. Geol. Soc. 165, 1045–1057.

Arboit, F., Min, M., Chew, D., Mitchell, A., Drost, K., Badenszki, E., Daly, J., 2021. Constraining the links between the Himalayan belt and the central Myanmar basins during the Cenozoic: an integrated multi-proxy detrital geochronology and trace-element geochemistry study. Geosci. Front. 12, 657–676.

Bayon, G., Toucanne, S., Skonieczny, C., Andre, L., Bermell, S., Cheron, S., Dennielou, B., Etoubleau, J., Freslon, N., Gauchery, T., Germain, Y., Jorry, S.J., Menot, G., Monin, L., Ponzevera, E., Rouget, M.L., Tachikawa, K., Barrat, J.A., 2015. Rare Earth elements and neodymium isotopes in world river sediments revisited. Geochim. Cosmochim. Acta 170, 17–38.

Bender, F., 1983. Geology of Burma. Bontraeger, Berlin.

Bertrand, G., Rangin, C., 2003. Tectonics of the western margin of the Shan plateau (central Myanmar): implication for the India–Indochina oblique convergence since the Oligocene. J. Asian Earth Sci. 21, 1139–1157.

Bertrand, G., Rangin, C., Maluski, H., Bellon, H., Party, G.S., 2001. Diachronous cooling along the Mogok Metamorphic Belt (Shan scarp, Myanmar): the trace of the northward migration of the Indian syntaxis. J. Asian Earth Sci. 19, 649–659.

Bodet, F., Schärer, U., 2000. Evolution of the SE-Asian continent from U–Pb and Hf isotopes in single grains of zircon and baddeleyite from large rivers. Geochim. Cosmochim. Acta 64, 2067–2091.

Bretschneider, L., Hathorne, E.C., Huang, H., Lübbers, J., Kochhann, K.G., Holbourn, A., Kuhnt, W., Thiede, R., Gebregiorgis, D., Giosan, L., 2021. Provenance and weathering of clays delivered to the Bay of Bengal during the middle Miocene: linkages to tectonics and monsoonal climate. J. Paleoceanogr. Paleoclimatol., e2020PA003917.

Colin, C., Turpin, L., Bertaux, J., Desprairies, A., Kissel, C., 1999. Erosional history of the Himalayan and Burman ranges during the last two glacial–interglacial cycles. Earth Planet. Sci. Lett. 171, 647–660.

Damodararao, K., Singh, S.K., Rai, V.K., Ramaswamy, V., Rao, P.S., 2016. Lithology, monsoon and sea-surface current control on provenance, dispersal and deposition of sediments over the Andaman continental shelf. Front. Mar. Sci. 3.

Gabriel, K.R., 1971. The biplot graphic display of matrices with application to principal component analysis. Biometrika 58, 453–467.

Galehouse, J.S., 1971. Point counting. In: Carver, R.E. (Ed.), Procedures in Sedimentary Geology. Wiley, New York, pp. 385–407.

Garçon, M., Chauvel, C., France-Lanord, C., Huyghe, P., Lavé, J., 2013. Continental sedimentary processes decouple Nd and Hf isotopes. Geochim. Cosmochim. Acta 121, 177–195.

Garzanti, E., Vezzoli, G., 2003. A classification of metamorphic grains in sands based on their composition and grade. J. Sediment. Res. 73, 830–837.

Garzanti, E., Wang, J.G., Vezzoli, G., Limonta, M., 2016. Tracing provenance and sediment fluxes in the Irrawaddy River basin (Myanmar). Chem. Geol. 440, 73–90.

Giosan, L., Naing, T., Tun, M.M., Clift, P.D., Filip, F., Constantinescu, S., Khonde, N., Blusztajn, J., Buylaert, J.P., Stevens, T., Thwin, S., 2018. On the Holocene evolution of the Ayeyawady megadelta. Earth Surf. Dyn. 6, 451–466.

Ingersoll, R.V., Bullard, T.F., Ford, R.L., Grimm, J.P., Pickle, J.D., Sares, S.W., 1984. The effect of grain size on detrital modes: a test of the Gazzi-Dickinson point-counting method. J. Sediment. Res. 54, 103–116.

Jaeger, J.-J., Soe, A.N., Chavasseau, O., Coster, P., Emonet, E.-G., Guy, F., Lebrun, R., Maung, A., Khyaw, A.A., Shwe, H., 2011. First hominoid from the late Miocene of the Irrawaddy Formation (Myanmar). PLoS ONE 6, e17065.

Khin, K., Myitta, 1999. Marine transgression and regression in Miocene sequences of northern Pegu (Bago) Yoma, Central Myanmar. J. Asian Earth Sci. 17, 369–393.

Lamont, T.N., Searle, M.P., Hacker, B.R., Htun, K., Htun, K.M., Morley, C.K., Waters, D.J., White, R.W., 2021. Late Eocene-Oligocene granulite facies garnet-sillimanite migmatites from the Mogok Metamorphic belt, Myanmar, and implications for timing of slip along the Sagaing Fault. Lithos, 386–387.

Liang, Y.H., Chung, S.L., Liu, D.Y., Xu, Y.G., Wu, F.Y., Yang, J.H., Wang, Y., Lo, C.H., 2008. Detrital zircon evidence from Burma for reorganization of the eastern Himalayan river system. Am. J. Sci. 308, 618–638.

Licht, A., Dupont-Nivet, G., Win, Z., Swe, H.H., Kaythi, M., Roperch, P., Ugrai, T., Littell, V., Park, D., Westerweel, J., Jones, D., Poblete, F., Aung, D.W., Huang, H., Hoorn, C., Sein, K., 2018. Paleogene evolution of the Burmese forearc basin and implications for the history of India-Asia convergence. Geol. Soc. Am. Bull. 131, 730–748.

Licht, A., France-Lanord, C., Reisberg, L., Fontaine, C., Soe, A.N., Jaeger, J.J., 2013. A palaeo Tibet–Myanmar connection? Reconstructing the Late Eocene drainage system of central Myanmar using a multi-proxy approach. J. Geol. Soc. 170, 929–939.

Licht, A., Reisberg, L., France-Lanord, C., Naing Soe, A., Jaeger, J.J., 2016. Cenozoic evolution of the central Myanmar drainage system: insights from sediment provenance in the Minbu Sub-Basin. Basin Res. 28, 237–251.

Licht, A., Win, Z., Westerweel, J., Cogne, N., Morley, C.K., Chantraprasert, S., Poblete, F., Ugrai, T., Nelson, B., Aung, D.W., Dupont-Nivet, G., 2020. Magmatic history of central Myanmar and implications for the evolution of the Burma Terrane. Gondwana Res. 87, 303–319.

Lin, T.H., Mitchell, A.H.G., Chung, S.L., Tan, X.B., Tangl, J.T., Oo, T., Wu, F.Y., 2019. Two parallel magmatic belts with contrasting isotopic characteristics from southern Tibet to Myanmar: zircon U–Pb and Hf isotopic constraints. J. Geol. Soc. Lond. 176, 574–587.

Maurin, T., Rangin, C., 2009. Structure and kinematics of the Indo-Burmese Wedge: recent and fast growth of the outer wedge. Tectonics 28 (2). https://doi.org/10.1029/2008TC002276.

Mitchell, A.H.G., 1993. Cretaceous–Cenozoic tectonic events in the western Myanmar (Burma)–Assam region. J. Geol. Soc. 150, 1089–1102.

Morley, C.K., Arboit, F., 2019. Dating the onset of motion on the Sagaing fault: evidence from detrital zircon and titanite U–Pb geochronology from the North Minwun Basin, Myanmar. Geology 47, 581–585.
Naing, T.T., Bussien, D.A., Winkler, W.H., Nold, M., Von Quadt, A., 2014. Provenance study on Eocene-miocene sandstones of the Rakhine Coastal Belt, Indo-Burman ranges of Myanmar: geodynamic implications. In: Sediment Provenance Studies in Hydrocarbon Exploration and Production, vol. 386, pp. 195–216.
Najman, Y., Sobel, E.R., Millar, I., Stockli, D.F., Govin, G., Lisker, F., Garzanti, E., Limonta, M., Vezzoli, G., Copley, A., Zhang, P., Szymanski, E., Kahn, A., 2020. The exhumation of the Indo-Burman Ranges, Myanmar. Earth Planet. Sci. Lett. 530.
Oo, K.L., Zaw, K., Sebastien, M., Myitta, Aung D.W., Lai, C.K., 2015. Provenance of the Eocene sandstones in the southern Chindwin Basin, Myanmar: implications for the unroofing history of the Cretaceous–Eocene magmatic arc. J. Asian Earth Sci. 107, 172–194.
Pivnik, D.A., Nahm, J., Tucker, R.S., Smith, G.O., Nyein, K., Nyunt, M., Maung, P.H., 1998. Polyphase deformation in a fore-arc/back-arc basin, Salin subbasin, Myanmar (Burma). Am. Assoc. Pet. Geol. Bull. 82, 1837–1856.
Ridd, M.F., Racey, A., 2015. Chapter 4 Onshore petroleum geology of Myanmar: central Burma depression. Mem. Geol. Soc. Lond. 45, 21–50.
Robinson, R.A.J., Bird, M.I., Oo, N.W., Hoey, T.B., Aye, M.M., Higgitt, D.L., Lu, X.X., Swe, A., Tun, T., Win, S.L., 2007. The Irrawaddy River sediment flux to the Indian Ocean: the original nineteenth-century data revisited. J. Geol. 115, 629–640.
Robinson, R.A.J., Brezina, C.A., Parrish, R.R., Horstwood, M.S.A., Oo, N.W., Bird, M.I., Thein, M., Walters, A.S., Oliver, G.J.H., Zaw, K., 2014. Large rivers and orogens: the evolution of the Yarlung Tsangpo-Irrawaddy system and the eastern Himalayan syntaxis. Gondwana Res. 26, 112–121.
Sloan, R.A., Elliott, J.R., Searle, M.P., Morley, C.K., 2017. Chapter 2 active tectonics of Myanmar and the Andaman Sea, vol. 48. Mem. Geol. Soc. Lond. 48, 19–52.
Socquet, A., Pubellier, M., 2005. Cenozoic deformation in western Yunnan (China-Myanmar border). J. Asian Earth Sci. 24, 495–515.
Soe Thura, T., Watkinson, I.M., 2017. Chapter 19 the sagaing fault, Myanmar. Mem. Geol. Soc. Lond. 48, 413–441.
Takai, M., Kusuhashi, N., Nishioka, Y., Thaung, H., Zin Maung Maung, T., 2018. Geological setting and transition of the Neogene mammal fauna in central Myanmar. Fossils: Palaeontol. Soc. Jpn. 103, 15.
Tang, R., 2013. Detrital Zircon Study of the Irrawaddy and Salween Rivers in Myanmar. National Taiwan University, Taipei.
Thein, M., Maung, M., 2017. Chapter 8 The Eastern (back-arc) basin of Central Myanmar: basement rocks, lithostratigraphic units, palaeocurrents, provenance and developmental history. Mem. Geol. Soc. Lond. 48, 169–183.
Vermeesch, P., Resentini, A., Garzanti, E., 2016. An R package for statistical provenance analysis. Sediment. Geol. 336, 14–25.
Wang, G., Wan, J.L., Wang, E.C., Zheng, D.W., Li, F., 2008. Late Cenozoic to recent transtensional deformation across the Southern part of the Gaoligong shear zone between the Indian plate and SE margin of the Tibetan Plateau and its tectonic origin. Tectonophysics 460, 1–20.
Wang, J.G., Wu, F.Y., Tan, X.C., Liu, C.Z., 2014. Magmatic evolution of the Western Myanmar Arc documented by U–Pb and Hf isotopes in detrital zircon. Tectonophysics 612, 97–105.
Westerweel, J., Licht, A., Cogné, N., Roperch, P., Dupont-Nivet, G., Kay Thi, M., Swe, H.H., Huang, H., Win, Z., Wa Aung, D., 2020. Burma Terrane collision and northward indentation in the Eastern Himalayas recorded in the Eocene-Miocene Chindwin Basin (Myanmar). Tectonics 39, e2020TC006413.
Zhang, B., Zhang, J., Zhong, D., Yang, L., Yue, Y., Yan, S., 2012. Polystage deformation of the Gaoligong metamorphic zone: structures, 40Ar/39Ar mica ages, and tectonic implications. J. Struct. Geol. 37, 1–18.
Zhang, P., Mei, L., Jiang, S.-Y., Xu, S., Donelick, R.A., Li, R., Zhang, H., 2021. Erosion and sedimentation in SE Tibet and Myanmar during the evolution of the Burmese continental margin from the late Cretaceous to early Neogene. Gondwana Res. 95, 149–175.
Zhang, P., Najman, Y., Mei, L.F., Millar, I., Sobel, E.R., Carter, A., Barfod, D., Dhuime, B., Garzanti, E., Govin, G., Vezzoli, G., Hu, X.L., 2019. Palaeodrainage evolution of the large rivers of East Asia, and Himalayan-Tibet tectonics. Earth-Sci. Rev. 192, 601–630.